



## ISTITUTO NAZIONALE DI RICERCA METROLOGICA Repository Istituzionale

Verification of Knoop indenters with a Vickers-addressed optical system

This is the author's accepted version of the contribution published as:

*Original*

Verification of Knoop indenters with a Vickers-addressed optical system / Prato, Andrea; Origlia, Claudio; Germak, Alessandro. - In: MEASUREMENT. - ISSN 0263-2241. - 163:(2020), p. art. no. 107928. [10.1016/j.measurement.2020.107928]

*Availability:*

This version is available at: 11696/62430 since: 2021-05-27T17:40:42Z

*Publisher:*

Elsevier

*Published*

DOI:10.1016/j.measurement.2020.107928

*Terms of use:*

This article is made available under terms and conditions as specified in the corresponding bibliographic description in the repository

*Publisher copyright*

(Article begins on next page)

1 **Verification of Knoop indenters with a Vickers-addressed optical**  
2 **system**

3  
4 *Andrea Prato<sup>1</sup>, Claudio Origlia<sup>1</sup> and Alessandro Germak<sup>1</sup>*

5  
6 *<sup>1</sup> INRiM - Istituto Nazionale di Ricerca Metrologica, 10135 Torino, Italy*

7  
8 Corresponding author e-mail: *a.prato@inrim.it*

9  
10 Abbreviated title: Knoop indenters verification with optical system

11  
12  
13  
14  
15  
16  
17  
18  
19  
20  
21  
22  
23  
24

25     **Abstract**

26     ISO 4545-2 and 4545-3 of Knoop hardness tests require the geometrical verification of the indenters. IN-  
27     RiM hardness laboratory, in cooperation with Galileo-LTF®, has developed the Gal-Indent optical measuring  
28     system for the verification of Vickers indenters. This system can measure the vertex angles between two op-  
29     posite faces, the quadrilateral base angles and the pyramid axis tilt angle. Using these measured quantities as  
30     inputs of a suitable geometrical model, the angles between the opposite edges at the vertex of Knoop indenters,  
31     nominally 172.5° and 130°, and the angle between the pyramid and indenter holder axes can be verified with  
32     an expanded uncertainty of 0.05°. Comparison of experimental measurements performed on three different  
33     Knoop indenters, previously verified by an accredited laboratory, shows compatible results. The proposed  
34     geometrical model could be easily implemented by laboratories that adopt similar measuring systems ad-  
35     dressed for the verification of Vickers indenters without any modification of the experimental apparatus.

36

37     **Keywords:** Hardness, Knoop indenter, Geometrical model, Gal-indent optical system.

38

39

40

41

42

43

44

45

46

47

48

49

50 **1. Introduction**

51 Knoop indenter is a pyramidal diamond with a rhombic quadrilateral base that produces an elongated indent.  
52 The angles between the opposite edges at the vertex of the diamond pyramid of the indenter,  $\alpha$  and  $\beta$ , are  
53  $172.5^\circ$  and  $130^\circ$ , respectively, and the ratio between long and short diagonals is approximately 7.11 to 1 (Fig.  
54 1). This entails that the angles of the rhombic base,  $\varphi_i$  and  $\tau_i$  ( $i=1,2$ ), are approximately  $164^\circ$  and  $16^\circ$ , respec-  
55 tively, and that the angles between the two opposite faces of the vertex  $\theta$  are approximately  $129.57^\circ$ .

56 These characteristics make Knoop hardness ideal for testing surface defects, brittle materials and small  
57 specimens, including thin metal films [1]. Moreover, due to the sensitivity of Knoop hardness to the indenter  
58 orientation, it is useful to evaluate the anisotropy of materials [2]. The influence of indenter characteristics on  
59 hardness measurements is largely reported in literature in particular for Vickers and Rockwell hardness. By  
60 performing the analysis of variances on a large set of Vickers and Rockwell tests, it was found that the geom-  
61 etry of the indenters was statistically significant in most of the cases [3] producing a relevant uncertainty  
62 contribution [4]. In Rockwell hardness, besides tip radius and cone angle, this can also be due to roughness,  
63 indenter deformations under load [5] or to the soldering of the diamond cone into the holder [6]. In addition,  
64 it was found that increasing the cone angle and the tip radius of the indenter entails an increase in Rockwell  
65 hardness value [7]. In Vickers hardness, on the contrary, it was found that an indenter with a larger angle,  
66 although within the limits allowed by the ISO standard, entails a wider indentation, thus a decrease in hardness  
67 value [8], which might exceed permissible values [9]. However for Knoop hardness, few studies on the influ-  
68 ence of the indenter geometry are found. One showed that small geometric imperfections of the indenters have  
69 a negligible influence on the contact area but a noticeable influence on the force–depth response [10]. Others  
70 showed that the influence of indenter geometry on hardness may not be negligible when testing enamels [11]  
71 and cobalt-based alloys [12]. Furthermore, in depth-sensing indentation, it was shown that the geometry of  
72 Knoop indenter affects the evaluation Young's modulus of the indented material [13], while, in nanoindentation,  
73 non-geometrically perfect Knoop indenters provide accurate results even at the very low loads at which  
74 a nanoindenter operates [14].

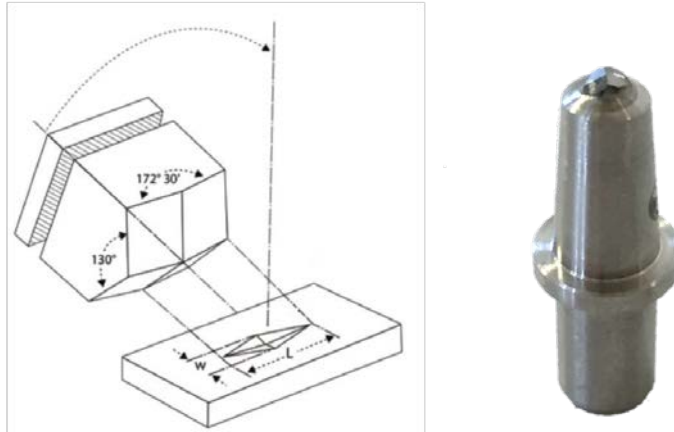
75 ISO 4545-2 and 4545-3 [15,16] specify the requirements of the indenters with different tolerances. The  
76 second is more restrictive since it refers to the calibration of reference blocks. The tolerance for the angle of

77 172.5° is  $\pm 0.1^\circ$  in both documents, whereas for the angle of 130° the tolerance is  $\pm 1^\circ$  and  $\pm 0.1^\circ$ , respectively.  
78 Furthermore, the angle  $\delta$  between the axis of the diamond pyramid and the axis of the indenter holder (normal  
79 to the seating surface), named tilt angle, shall not exceed 0.5° and 0.3°, respectively. The four faces of the  
80 diamond pyramid shall also be polished and free from surface defects and the indenter constant  
81  $c = \tan(\beta/2) / (2 \tan(\alpha/2))$  shall be within 1,0 % of the ideal value 0.07028, i.e.  $0.06958 \leq c \leq 0.07098$ . In addition,  
82 the device used for the verification shall have a maximum expanded uncertainty of 0.07°.

83 At present, verification of Knoop hardness is performed by few manufacturers and laboratories that own  
84 specific instrumentation addressed for the scope. Conversely, verification of squared-based Vickers indenters,  
85 based on the measurement of the angles between the opposite faces of the vertex, the squareness of the quad-  
86 rilateral base angles and the angle between the axis of the diamond pyramid and the axis of the indenter holder,  
87 can be performed by a larger number of calibration laboratories and industries with dedicated systems. Given  
88 the similar geometry of the two indenters, in this paper it is investigated the possibility to use Vickers-ad-  
89 dressed systems for the verification of Knoop indenters by implementing a simple geometrical model, in order  
90 to extend the measurement capability of these laboratories without changing the experimental apparatus or  
91 developing new ones.

92 Verification of Vickers indenters is usually performed with optical measuring systems using scanning in-  
93 terferometry [17], microscopes [18] or scanning confocal probes [19]. INRiM hardness laboratory, in cooper-  
94 ation with Galileo-LTF® [20,21], has developed a specific optical measuring system (commercialized by the  
95 Galileo-LTF® as Gal-Indent) for the verification of the geometry of Vickers indenters [22]. This system is  
96 able to directly measure the main geometrical parameters of Vickers indenters required by the standard, i.e.  
97 the two vertex angles between two opposite faces, the four angles of the square base, and the angle between  
98 the axis of the diamond pyramid and the axis of the indenter holder, with an expanded uncertainty of 0.05°.  
99 By measuring these quantities for Knoop indenters and with a suitable geometrical model, the possibility to  
100 evaluate their geometrical parameters required by the relevant Standards is investigated. This paper deals with  
101 a brief description of the Gal-Indent optical system (Section 2), the geometrical model (Section 3) and a com-  
102 parison of experimental results among three different Knoop indenters with values obtained by a German ac-  
103 credited laboratory to validate the proposed method (Section 4).

104



105

106

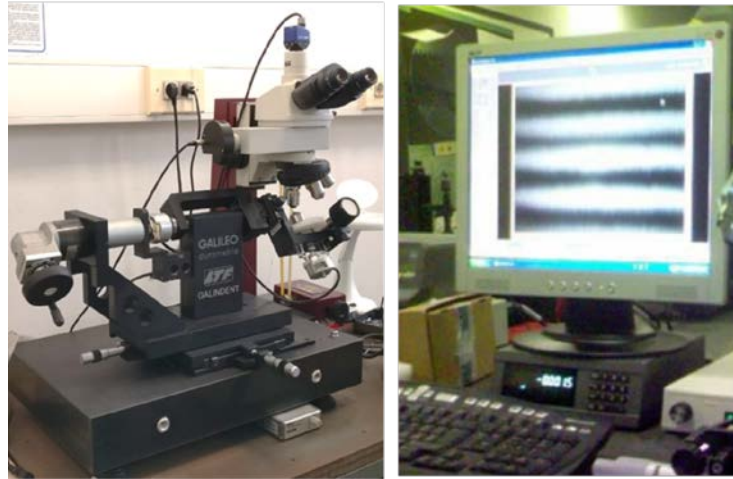
**Fig. 1.** Schematic draw (left) [23] and picture (right) of a Knoop indenter.

## 107 2. The Gal-Indent optical system

108 In INRiM hardness laboratory a specific measuring system, commercialized by Galileo-LTF® as Gal-Inden-  
 109 dent optical system (Fig. 2), was developed and is currently used for the verification of Vickers indenters. The  
 110 system is also adopted by different National Metrological Institutes (NMIs) and calibration laboratories around  
 111 the world. It is able to measure the vertex angle of the indenter between two opposite faces, and the quadrilat-  
 112 eral base angles by means of two angular encoders [24]. The optical system is based on Mirau interferometry.  
 113 A green laser beam with a wavelength of 546 nm, emitted by a light source, is divided in two beams: the first  
 114 reaches the observer through the eyepiece and the second strikes the surface of the indenter and is reflected  
 115 back creating an interference pattern. Through a mechanical system, the indenter is simultaneously rotated  
 116 around the indenter-holder axis and around the axis parallel to the plane of the microscope lens passing through  
 117 the diamond pyramid vertex until the number of interference fringes is minimized, thus obtaining a lateral  
 118 indenter face parallel to the microscope lens. These two rotations are measured by means of two angular en-  
 119 coders. The first rotation, around the indenter-holder axis, represents the measurement of quadrilateral base  
 120 angles. The second rotation around the axis parallel to the plane of the lens represents the measurement of the  
 121 supplementary angles of each lateral face from which the angles between two opposite faces and the angle  
 122 between the axis of the diamond pyramid and the axis of the indenter holder are obtained [25], as required for

123 the verification of Vickers indenters. Using these measurements as input of a suitable geometrical model, pre-  
124 sented in the following Section, the possibility to evaluate the geometrical parameters of Knoop indenters is  
125 investigated.

126



127

128

**Fig. 2.** The Galileo-LTF® Gal-Indent optical system.

129

### **3. The geometrical model**

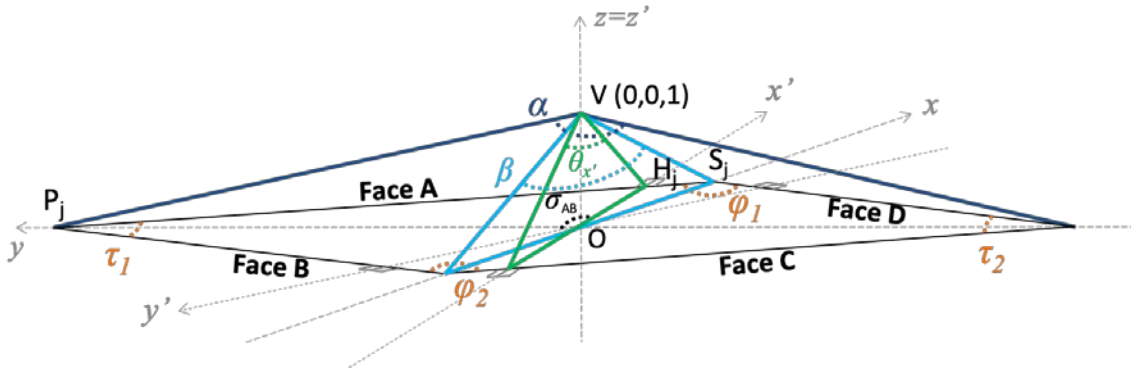
130

#### *3.1 Evaluation of the tilt angle*

131

The geometry of an ideal Knoop indenter, i.e. an indenter with four generic faces (A, B, C, D), with angles  
132 between the opposite edges at the vertex of the diamond pyramid  $\alpha$  and  $\beta$  equal to  $172.5^\circ$  and  $130^\circ$ , respec-  
133 tively, with angles  $\theta$  between two opposite faces equal to  $129.57^\circ$ , and with a tilt angle  $\delta$  equal to  $0^\circ$ , is sche-  
134 matically depicted in Fig. 3.  $xyz$  and  $x'y'z'$  coordinate systems correspond, respectively, to the diagonals of the  
135 Knoop indenter rhombic base, and to the optical reference system that is perpendicular to the perimeter of two  
136 opposite faces. Therefore, the angle between  $x$ - and  $y$ -axis is nominally  $90^\circ$ , whereas the angle  $\sigma_{AB}$  between  $x'$ -  
137 and  $y'$ -axis is nominally  $164^\circ$ . For each  $j$ -th face ( $j=A, B, C, D$ ), the intersection between an optical reference  
138 axis ( $x'$ - or  $y'$ -axis) and the base perimeter is identified by point  $H_j$ , whereas the intersection with  $x$ - and  $y$ -axis  
139 are identified by points  $S_j$  and  $P_j$ , respectively (thus  $S_A=S_D, S_B=S_C, P_A=P_B, P_C=P_D$ ). The pyramid vertex  $V$  is  
140 arbitrarily placed on  $z=1$ . A cross-section of an ideal Knoop indenter along  $x'z'$  optical system plane is also  
141 shown in Fig. 4. The quadrilateral base angles  $\varphi_i$  and  $\tau_i$  ( $i=1,2$ ), nominally  $164^\circ$  and  $16^\circ$ , respectively, and the

142 supplementary angles of each  $j$ -th lateral face (A, B, C, D) along  $x'$  and  $y'$ -axis,  $\omega_j$ , nominally  
 143  $(180^\circ-129.57^\circ)/2 \approx 25.22^\circ$ , are measured by means of the optical system previously described.

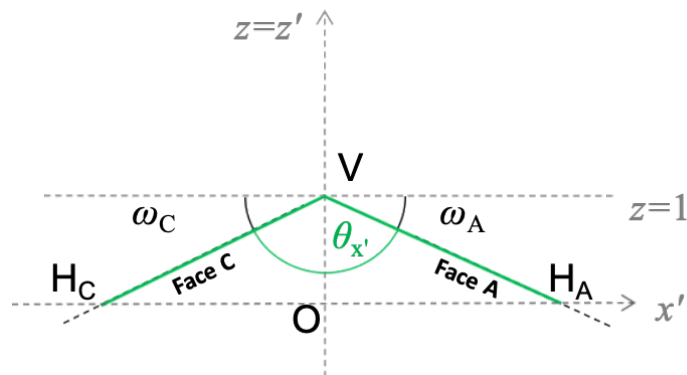


144

145

**Fig. 3.** 3-D schematic representation of an ideal Knoop indenter rhombic-based pyramid.

146



147

148

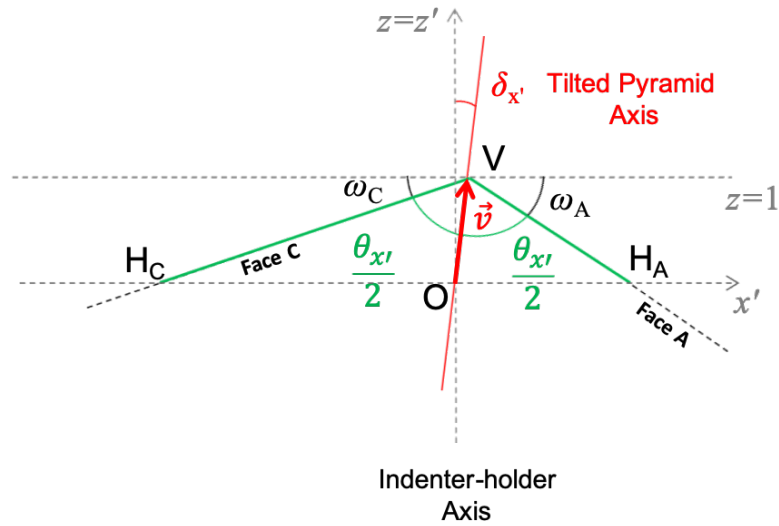
**Fig. 4.** Cross-section of an ideal Knoop indenter along  $x'z'$  optical reference system plane.

149

150 However, in real Knoop indenters, the tilt angle  $\delta$  between the axis of the diamond pyramid  $\mathbf{v}=\overline{OV}=(v_x, v_y, v_z)$   
 151 and the axis of the indenter holder angle ( $z'$ -axis) is not exactly  $0^\circ$ , thus an angle  $\gamma$  between the projection of  
 152 the pyramid vertex on  $z=0$  plane and  $x'$ -axis appears, as shown in Fig. 5.

153





170

171

**Fig. 6.** Cross-section of a real Knoop indenter along  $x'z'$  optical reference system plane.

172

173

By projecting the pyramid tilted axis vector  $\mathbf{v}$  along non-orthogonal  $x'z'$  and  $y'z'$  planes, according to Fig. 7

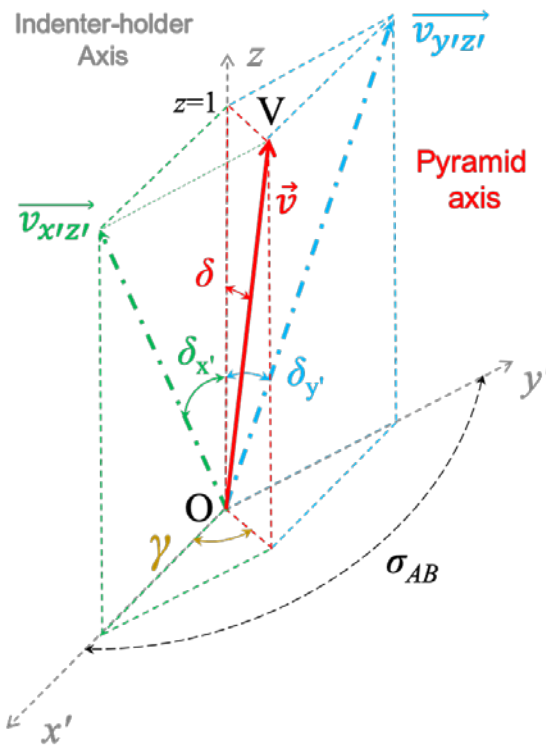
174

and Fig. 8, Eq. (5) is derived. Successively, implementing the equations of non-orthogonal systems (Fig. 9)

175

and using Eq. (5), Eqs. (6)-(8) and Eqs. (9)-(10) can be derived.

176

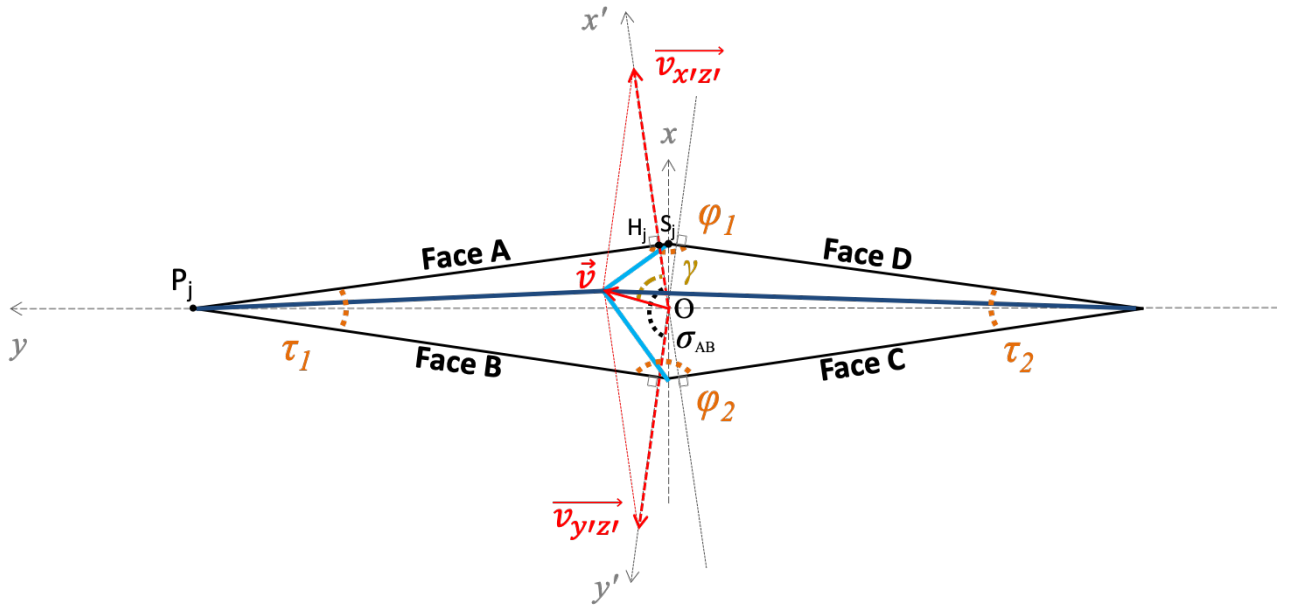


177

178

**Fig. 7.** Projection of Knoop indenter axis  $\mathbf{v}$  along  $x'$ - and  $y'$ - axis.

179

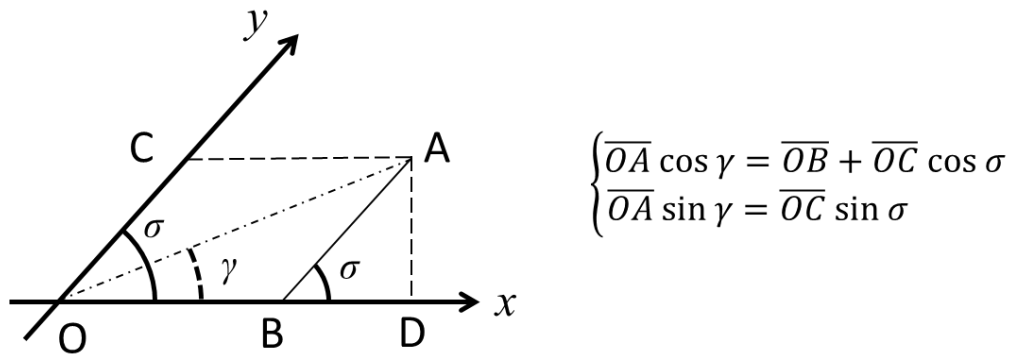


180

181

**Fig. 8.** Upper view of a real Knoop indenter with axis vector  $\mathbf{v}$  and its projections along  $x'$ - and  $y'$ - axis.

182



183

184

**Fig. 9.** Generic non-orthogonal reference system with relevant equations.

185

$$\|\mathbf{v}\| \cos \delta = \|\mathbf{v}_{x'z'}\| \cos \delta_{x'} = \|\mathbf{v}_{y'z'}\| \cos \delta_{y'} \quad (5)$$

186

$$\begin{aligned} \|\mathbf{v}\| \sin \delta \cos \gamma &= \|\mathbf{v}_{x'z'}\| \sin \delta_{x'} + \|\mathbf{v}_{y'z'}\| \sin \delta_{y'} \cos \sigma_{AB} = \\ &= \|\mathbf{v}\| \frac{\cos \delta}{\cos \delta_{x'}} \sin \delta_{x'} + \|\mathbf{v}\| \frac{\cos \delta}{\cos \delta_{y'}} \sin \delta_{y'} \cos \sigma_{AB} \end{aligned} \quad (6)$$

$$\sin \delta \cos \gamma = \frac{\cos \delta}{\cos \delta_{x'}} \sin \delta_{x'} + \frac{\cos \delta}{\cos \delta_{y'}} \sin \delta_{y'} \cos \sigma_{AB} \quad (7)$$

$$\tan \delta \cos \gamma = \tan \delta_{x'} + \tan \delta_{y'} \cos \sigma_{AB} \quad (8)$$

$$\|\mathbf{v}\| \sin \delta \sin \gamma = \|\mathbf{v}_{y'z'}\| \sin \delta_{y'} \sin \sigma_{AB} = \|\mathbf{v}\| \frac{\cos \delta}{\cos \delta_{y'}} \sin \delta_{y'} \sin \sigma_{AB} \quad (9)$$

$$\tan \delta \sin \gamma = \tan \delta_{y'} \sin \sigma_{AB} \quad (10)$$

187 By performing the squared sum of Eqs. (8) and (10), the total tilt angle  $\delta$  can be obtained (see Eqs. (11)-(13)):

188

$$\tan^2 \delta \cos^2 \gamma + \tan^2 \delta \sin^2 \gamma = \tan^2 \delta_{x'} + \tan^2 \delta_{y'} \cos^2 \sigma_{AB} + 2 \tan \delta_{x'} \tan \delta_{y'} \cos \sigma_{AB} + \tan^2 \delta_{y'} \sin^2 \sigma_{AB} \quad (11)$$

$$\tan^2 \delta = \tan^2 \delta_{x'} + \tan^2 \delta_{y'} + 2 \tan \delta_{x'} \tan \delta_{y'} \cos \sigma_{AB} \quad (12)$$

$$\delta = \arctan \sqrt{\tan^2 \delta_{x'} + \tan^2 \delta_{y'} + 2 \tan \delta_{x'} \tan \delta_{y'} \cos(\sigma_{AB})} \quad (13)$$

189 and from the ratio between Eqs. (10) and (8), the angle  $\gamma$  can be derived (see Eqs. (14)-(15)):

$$\tan \gamma = \frac{\tan \delta_{y'} \sin \sigma_{AB}}{\tan \delta_{x'} + \tan \delta_{y'} \cos \sigma_{AB}} \quad (14)$$

$$\gamma = \arctan \left( \frac{\tan \delta_{y'} \sin \sigma_{AB}}{\tan \delta_{x'} + \tan \delta_{y'} \cos \sigma_{AB}} \right) \quad (15)$$

190

### 191 3.2 Evaluation of the angles between the opposite edges at the vertex

192 From the scheme of Fig. 5 and reminding that the pyramid vertex V is placed on  $z=1$ , the vector of the tilted  
 193 pyramid axis  $\mathbf{v}$  referred to the  $xyz$  reference system can be written according to Eq. (16), where  $\rho$  is the mean  
 194 angle between  $x'$ - and  $x$ -axis (see Eq. (2)).

195

$$\mathbf{v} = [\tan(\delta) \cos(\gamma + \rho), \tan(\delta) \sin(\gamma + \rho), 1] \quad (16)$$

196

197 Considering the triangle  $\text{OH}_j\text{V}$  in Fig. 5 and Fig. 6 for each  $j$ -th indenter face (A, B, C, D), given that  
 198  $\widehat{\text{OH}_j\text{V}} = \omega_j$ , and implementing the law of sines, Eq. (17) is obtained:

$$\overline{\text{OH}}_j = \|\mathbf{v}\| \frac{\sin \frac{\theta_j}{2}}{\sin \omega_j} \quad (17)$$

199 where  $\theta_A = \theta_C = \theta_x$  and  $\theta_B = \theta_D = \theta_y$ .

200 In this way, Eqs. (18) and (19) can be derived. The sign of the vector components for the four faces follows  
 201 the position on the  $xyz$  reference system as in Fig. 5.

$$\mathbf{OS}_j = \left( \frac{\overline{\text{OH}}_j}{\cos \rho_j}, 0, 0 \right) \quad (18)$$

$$\mathbf{OP}_j = \left( 0, \frac{\overline{\text{OH}}_j}{\sin \rho_j}, 0 \right) \quad (19)$$

202 Considering the triangle  $\text{OVS}_j$ , it is obtained that

$$\widehat{\text{VOS}}_j = \arccos \left( \frac{\mathbf{OS}_j \cdot \mathbf{v}}{\|\mathbf{v}\| \|\mathbf{OS}_j\|} \right) \quad (20)$$

203 Again, by applying the law of sines to triangle  $\text{OVS}_j$ , it is obtained that

$$\frac{\|\mathbf{v}\|}{\sin \widehat{\text{OS}}_j\text{V}} = \frac{\|\mathbf{OS}_j\|}{\sin \widehat{\text{OVS}}_j} = \frac{\|\mathbf{VS}_j\|}{\sin \widehat{\text{VOS}}_j} \quad (21)$$

204 Given that  $\widehat{\text{OS}}_j\text{V} = 180 - \widehat{\text{OVS}}_j - \widehat{\text{VOS}}_j$  and with some trigonometric calculations, Eq. (22) is obtained.

205

$$\sin \widehat{\text{OS}}_j\text{V} = \sin(180 - \widehat{\text{OVS}}_j - \widehat{\text{VOS}}_j) = \sin \widehat{\text{OVS}}_j \cos \widehat{\text{VOS}}_j + \sin \widehat{\text{VOS}}_j \cos \widehat{\text{OVS}}_j \quad (22)$$

206 In this way, combining Eq. (21) and Eq.(22), Eqs. (23)-(25) are obtained:

207

$$\frac{\|\mathbf{v}\|}{\|\mathbf{OS}_j\|} = \frac{\sin \widehat{\text{OS}}_j\text{V}}{\sin \widehat{\text{OVS}}_j} \quad (23)$$

$$\frac{\|\mathbf{v}\|}{\|\mathbf{OS}_j\|} = \frac{\sin \widehat{OVS}_j \cos \widehat{VOS}_j + \sin \widehat{VOS}_j \cos \widehat{OVS}_j}{\sin \widehat{OVS}_j} \quad (24)$$

$$\frac{\|\mathbf{v}\|}{\|\mathbf{OS}_j\|} = \cos \widehat{VOS}_j + \frac{\sin \widehat{VOS}_j}{\tan \widehat{OVS}_j} \quad (25)$$

208 and from Eq. (25), Eq. (26) is also obtained:

$$\widehat{OVS}_j = \arctan \left( \frac{\|\mathbf{OS}_j\| \sin \widehat{VOS}_j}{\|\mathbf{v}\| - \|\mathbf{OS}_j\| \cos \widehat{VOS}_j} \right) \quad (26)$$

209

210 By applying the same calculations from Eq. (20) onward to triangle  $VOP_j$ , it is found that,

211

$$\widehat{OVP}_j = \arctan \left( \frac{\|\mathbf{OP}_j\| \sin \widehat{VOP}_j}{\|\mathbf{v}\| - \|\mathbf{OP}_j\| \cos \widehat{VOP}_j} \right) \quad (27)$$

212

213 Therefore, considering a single  $j$ -th indenter face, the angles between two opposite edges can be found  
214 according to:

215

$$\alpha_j = 2 \widehat{OVP}_j \quad (28)$$

$$\beta_j = 2 \widehat{OVS}_j \quad (29)$$

216 Averaging the results obtained for each  $j$ -th indenter face, the angles between two opposite edges, nominally

217  $172.5^\circ$  (Eq. 30) and  $130^\circ$  (Eq. 31), are finally obtained:

218

$$\alpha = \frac{\sum_{j=1}^4 \alpha_j}{4} \quad (30)$$

$$\beta = \frac{\sum_{j=1}^4 \beta_j}{4} \quad (31)$$

219 **4. Comparison of experimental measurements**

220 In order to validate the geometrical model, experimental measurements were performed on three different  
 221 Knoop indenters previously verified by a German DKD accredited laboratory having comparable measurement  
 222 uncertainties. Calibration certificates data with expanded uncertainties at a confidence level of 95% are re-  
 223 ported in Table 1. Verification of the Knoop indenters' geometrical parameters was performed with the Gali-  
 224 leo-LTF® Gal-Indent optical system at INRiM. Experimental results with expanded uncertainties at a confi-  
 225 dence level of 95% (CMCs declared in the CIPM-MRA database) are reported in Table 2. In this way, by  
 226 applying the geometrical model of Section 3, the complete set of values required for the verification of the  
 227 Knoop indenters are obtained and summarized in Table 3. Expanded uncertainties (at a confidence level of  
 228 95%,  $k=2$ ), evaluated according to GUM [26] by propagating the experimental uncertainties, are in the order  
 229 of  $0.05^\circ$ , thus below the maximum expanded uncertainty of  $0.07^\circ$  required by the Standard. By way of exam-  
 230 ple, the detailed uncertainty budget for the angle between the opposite edges  $\beta$  of Knoop indenter 1 is shown  
 231 in Table 4.

232

233 **Table 1**

234 Calibration certificate values of the three tested Knoop indenters.

|   | <i>Knoop indenter 1</i> | <i>Knoop indenter 2</i> | <i>Knoop indenter 3</i> |
|---|-------------------------|-------------------------|-------------------------|
| <i>ID number</i>  | 3522                    | 3528                    | 3521                    |
| <i>Angle between the op-<br/>posite edges <math>\alpha /^\circ</math></i> | $172.53 \pm 0.03$       | $172.50 \pm 0.03$       | $172.50 \pm 0.03$       |
| <i>Angle between the op-<br/>posite edges <math>\beta /^\circ</math></i>  | $130.13 \pm 0.07$       | $129.83 \pm 0.07$       | $130.02 \pm 0.07$       |
| <i>Tilt angle <math>\delta /^\circ</math></i>                             | $<0.42 \pm 0.07$        | $<0.42 \pm 0.07$        | $<0.42 \pm 0.07$        |
| <i>Numerical factor <math>c / -</math></i>                                | $0.07018 \pm 0.00030$   | $0.07001 \pm 0.00030$   | $0.07031 \pm 0.00030$   |

235

236

237

**Table 2**

238

Experimental measurements on the three tested Knoop indenters.

|                      | <i>Knoop indenter 1</i> | <i>Knoop indenter 2</i> | <i>Knoop indenter 3</i> |
|----------------------|-------------------------|-------------------------|-------------------------|
| $\omega_A / ^\circ$  | $25.146 \pm 0.05$       | $25.297 \pm 0.05$       | $25.197 \pm 0.05$       |
| $\omega_B / ^\circ$  | $25.151 \pm 0.05$       | $25.275 \pm 0.05$       | $25.184 \pm 0.05$       |
| $\omega_C / ^\circ$  | $25.151 \pm 0.05$       | $25.310 \pm 0.05$       | $25.193 \pm 0.05$       |
| $\omega_D / ^\circ$  | $25.152 \pm 0.05$       | $25.278 \pm 0.05$       | $25.174 \pm 0.05$       |
| $\varphi_1 / ^\circ$ | $165.03 \pm 0.06$       | $163.86 \pm 0.06$       | $163.48 \pm 0.06$       |
| $\tau_1 / ^\circ$    | $16.07 \pm 0.06$        | $16.05 \pm 0.06$        | $15.43 \pm 0.06$        |
| $\varphi_2 / ^\circ$ | $163.01 \pm 0.06$       | $164.23 \pm 0.06$       | $164.56 \pm 0.06$       |
| $\tau_2 / ^\circ$    | $15.90 \pm 0.06$        | $15.86 \pm 0.06$        | $16.53 \pm 0.06$        |

239

240

**Table 3**

241

Geometrical parameters of the three tested Knoop indenters evaluated with the geometrical model.

|  | <i>Knoop indenter 1</i> | <i>Knoop indenter 2</i> | <i>Knoop indenter 3</i> |
|--|-------------------------|-------------------------|-------------------------|
| <i>ID number</i>   | 3522                    | 3528                    | 3521                    |
| <i>Angle between the opposite edges <math>\alpha / ^\circ</math></i> | $172.53 \pm 0.05$       | $172.50 \pm 0.05$       | $172.52 \pm 0.05$       |
| <i>Angle between the opposite edges <math>\beta / ^\circ</math></i>  | $130.13 \pm 0.05$       | $129.85 \pm 0.05$       | $130.06 \pm 0.05$       |
| <i>Tilt angle <math>\delta / ^\circ</math></i>                       | $0.09 \pm 0.05$         | $0.03 \pm 0.05$         | $0.06 \pm 0.05$         |
| <i>Numerical factor <math>c / -</math></i>                           | $0.07019 \pm 0.00048$   | $0.07007 \pm 0.00047$   | $0.07019 \pm 0.00048$   |

242 **Table 4**  
 243 Uncertainty budget for the angle between the opposite edges  $\beta$  of Knoop indenter 1.

| Variable $x_k$ |        |      | $u^2(x_k)$ | $c_k$                  | $u_k^2(a_x)$ | Rank |
|----------------|--------|------|------------|------------------------|--------------|------|
| Symbol         | Value  | Note |            |                        |              |      |
| $\omega_A$     | 25.146 | CMC  | 6,4E-04    | -5,1E-01               | 1,7E-04      | 1    |
| $\omega_B$     | 25.151 | CMC  | 6,4E-04    | -5,1E-01               | 1,7E-04      | 2    |
| $\omega_C$     | 25.151 | CMC  | 6,4E-04    | -5,1E-01               | 1,7E-04      | 3    |
| $\omega_D$     | 25.152 | CMC  | 6,4E-04    | -5,1E-01               | 1,7E-04      | 4    |
| $\varphi_1$    | 165.03 | CMC  | 9,1E-04    | -1,3E-02               | 1,5E-07      | 5    |
| $\tau_1$       | 16.07  | CMC  | 9,1E-04    | +1,3E-02               | 1,7E-07      | 6    |
| $\varphi_2$    | 163.01 | CMC  | 9,1E-04    | -1,3E-02               | 1,5E-07      | 7    |
| $\tau_2$       | 15.90  | CMC  | 9,1E-04    | +1,3E-02               | 1,7E-07      | 8    |
| $\beta$        | 130.13 |      |            | Variance, $u^2(\beta)$ | 6,6E-04      |      |
|                |        |      |            | St. unc. $u(\beta)$    | 2,6E-02      |      |

244  
 245 An analysis based on the estimation of the normalized error ( $E_n$ ) has been performed in order to assess the  
 246 compatibility of the experimental measurements performed at INRiM with respect to calibration certificate  
 247 values of the accredited laboratory, considered as reference.  $E_n$  is defined as the ratio of the difference between  
 248 the measured value ( $x$ ) and the reference value ( $y$ ) compared to the root sum square of associated expanded  
 249 uncertainties ( $U_x$  and  $U_y$ ) at a confidence level of 95 % ( $k = 2$ ). According to ISO/IEC 17043:2010 [27], it is  
 250 evaluated as follows:

$$E_n = \frac{|x-y|}{\sqrt{U_x^2 + U_y^2}} \quad (33)$$

251  
 252 Data can be considered compatible when  $E_n < 1$ . This is an indicator of accuracy/inaccuracy as compared  
 253 to an assigned reference value with respect to the associated uncertainties.

254 Combining data in Table 1 and Table 3, it is found that  $E_n$  is less than 1 for all geometrical parameters as  
 255 shown in Table 5. For tilt angle  $\delta$ , since the calibration certificates report only that the values fall below the  
 256 limit imposed by the standard, it is not possible to provide the exact normalized error. However, also experi-  
 257 mental results show values below the standard limits. Given such evidence, the proposed method provides  
 258 measurements compatible with the accredited laboratory.

259  
 260

261 **Table 5**262 Normalized errors  $E_n$  evaluated for the three tested Knoop indenters.

|   | <i>Knoop indenter 1</i> | <i>Knoop indenter 2</i> | <i>Knoop indenter 3</i> |
|---|-------------------------|-------------------------|-------------------------|
| <i>Angle between the opposite edges <math>\alpha</math></i> | 0.03                    | 0.06                    | 0.46                    |
| <i>Angle between the opposite edges <math>\beta</math></i>  | 0.04                    | 0.19                    | 0.33                    |
| <i>Numerical factor <math>c</math></i>                      | 0.02                    | 0.11                    | 0.21                    |

263

264 **5. Conclusions**

265 ISO 4545-2 and 4545-3 of Knoop hardness tests require the geometrical verification of the indenter. At  
266 present, verification of Knoop hardness is performed by few manufacturers and laboratories that use specific  
267 instrumentation for the purpose. Since the verification of Vickers indenters can be performed by a larger num-  
268 ber of calibration laboratories and industries with dedicated systems and given the similar geometry of the two  
269 indenters, the possibility to use Vickers-addressed systems for the verification of Knoop indenters, in order to  
270 extend the measurement capability of these laboratories, is investigated. These systems are usually based on  
271 optical measurements using microscopes, scanning interferometry or confocal probes. INRiM hardness labor-  
272 atory, in particular, uses a specific optical measuring system, based on Mirau interferometry, developed in  
273 cooperation with Galileo-LTF® and commercialized by Galileo-LTF® as Gal-Indent. It is able to measure the  
274 two vertex angles of the indenter between two opposite faces, the quadrilateral base angles and the angle be-  
275 tween the axis of the diamond pyramid and the axis of the indenter holder. This paper deals with the possibility  
276 to use such quantities as inputs of a suitable geometrical model in order to verify the geometry of Knoop  
277 indenters, i.e. to evaluate the angles between the opposite edges at the vertex, nominally  $172.5^\circ$  and  $130^\circ$ , and  
278 the angle between the axis of the diamond pyramid and the axis of the indenter holder, nominally  $0^\circ$ . The  
279 proposed geometrical model is described in Section 3. Experimental measurements, together with the associ-  
280 ated expanded uncertainties, were performed on three different Knoop indenters, previously measured by a

281 German DKD accredited laboratory, to verify the reliability of the model. Results of this work allow to high-  
282 light the following points:

- 283 • Using Vickers-addressed measured quantities as input of the proposed geometrical model allows  
284 to verify the geometry of Knoop indenters as requested by the relevant Standard.
- 285 • Comparison of measurement data with reference values shows compatible results in terms of nor-  
286 malized error, thus validating the proposed procedure.
- 287 • Expanded uncertainties are in the order of  $0.05^\circ$ , thus below the maximum expanded uncertainty  
288 of  $0.07^\circ$  required by the Standard.
- 289 • The advantage of this geometrical model is that it can be easily implemented, even on common  
290 spreadsheets, and exploited by laboratories that adopt similar measuring systems addressed for the  
291 verification of Vickers indenters without any modification of the experimental apparatus.

## 292 **References**

- 293 [1] F. Knoop, C. C. Peters, W. B. Emerson, A sensitive pyramidal diamond tool for indentation measurements,  
294 *Journal of Research of the National Bureau of Standards* 23 (1939) 39-61.
- 295 [2] J. Borc, Study of Knoop microhardness anisotropy on the (001), (100) and (010) faces of gadolinium cal-  
296 cium oxyborate single crystals, *Mater. Chem. Phys.* 148 (2014) 680–685.
- 297 [3] F. Petik, Problems of hardness measurement, *Measurement* 1(1) (1983) 24–30.
- 298 [4] G. Barbato, F. Petik, Metrological involvement in the definition and dissemination of hardness scales, in:  
299 *Proceedings of XIII IMEKO*, vol. 1, Torino, 1994, pp. 761–766.
- 300 [5] G. Barbato, M. Galetto, A. Germak, F. Mazzoleni, Influence of the indenter shape in Rockwell hardness  
301 test, in: *Proceedings of the HARDMEKO '98*, September 21–23, Beijing, China, 1998, pp. 53–60.
- 302 [6] R.S. Marriner, J.G. Wood, Investigation into the measurement and performance of Rockwell C diamond  
303 indenters, *Metallurgia* 87 (1967) 87–90.
- 304 [7] G. Barbato, S. Desogus, R. Levi, The meaning of the geometry of Rockwell indenters, *IMGC Tech. Rep.*  
305 R128 (1978).

- 306 [8] L. Brice, The influence of indenter characteristics on hardness measurements, in: Proceedings of XVII  
307 IMEKO World Congress Metrology, Dubrovnik, Croatia, June 22-27, 2003.
- 308 [9] M. El-Sherbiny, R. Hegazy, M. Ibrahim, and A. Abuelezz, The influence of geometrical tolerances of  
309 Vickers indenter on the accuracy of measured hardness, *Int. J. Metrol. Qual. Eng.* 3 (2012) 1–6.
- 310 [10] A.E. Giannakopoulos, Elastic and viscoelastic indentation of flat surfaces by pyramid indentors, *Journal*  
311 *of the Mechanics and Physics of Solids* 54 (2006) 1305–1332.
- 312 [11] C. Chuenarrom, P. Benjakul, P. Daosodsai, Effect of indentation load and time on Knoop and Vickers  
313 microhardness tests for enamel and dentin, *Materials Research* 12(4) (2009) 473-476.
- 314 [12] K. Sangwal, B. Surowskab, P. Błaziak, Analysis of the indentation size effect in the microhardness  
315 measurement of some cobalt-based alloys, *Materials Chemistry and Physics* 77 (2002) 511–520.
- 316 [13] M. I. Simões, J. M. Antunes, J. V. Fernandes, N. A. Sakharova, Numerical simulation of the depth-sensing  
317 indentation test with Knoop indenter, *Metals* 8 (2018) 885.
- 318 [14] L. Riestler, P.J. Blaua, E. Lara-Curzioa, K. Brederb, Nanoindentation with a Knoop indenter, *Thin Solid*  
319 *Films* 377-378 (2000) 635-639.
- 320 [15] ISO 4545:2017-2 Metallic materials — Knoop hardness test — Verification and calibration of testing  
321 machines.
- 322 [16] ISO 4545:2017-3 Metallic materials — Knoop hardness test — Calibration of reference blocks.
- 323 [17] S. Takagi, K. Kamijo, T. Usuda, H. Kawachi, K. Hanaki, Wide-range verification of the geometry of  
324 Vickers diamond indenters, in: Proceedings of XVIII IMEKO World Congress Measurement, Rio de Janeiro,  
325 Brazil, September 17-22, 2006.
- 326 [18] K. Hasche, K. Herrmann, F. Pohlenz, K. Thiele, Determination of the geometry of microhardness indent-  
327 ers with a scanning force microscope, *Meas. Sci. Technol.* 9 (1998) 1082–1086.
- 328 [19] T. Sanponpute, W. Limthunyalak, F. Menelao, D. Schwenk, Vickers indenter shape measurement by  
329 using scanning confocal chromatic instrument, in: Proceedings of XXI IMEKO World Congress “Measure-  
330 ment in Research and Industry”, Prague, Czech Republic, August 30 - September 4, 2015.

- 331 [20] G. Barbato, G. Gori, Metrological references in Hardness Measurement: a necessary background for in-  
332 dustrial Quality Assurance, In: Proceedings of the 5th Congreso Nacional de Metrologia Industrial, Zaragoza,  
333 Spain, 13-15 November, 1991, pp. 139-149.
- 334 [21] G. Barbato, S. Desogus, Measurement of the spherical tip of Rockwell indenters, Journal of Testing and  
335 Evaluation 16(4) (1988) 369-374.
- 336 [22] A. Liguori, A. Germak, G. Gori, E. Messina, Galindent: the reference metrological system for the verifi-  
337 cation of the geometrical characteristics of Rockwell and Vickers diamond indenters, In: VDI/VDE-GMA,  
338 IMEKO TC3/TC5/TC20 Joint International Conference, 24-26 Sept. 2002, VDI-Berichte 1685, Tagung Celle,  
339 Germany, 2002, pp. 365-371.
- 340 [23] F.C. Campbell, Inspection of Metals: Understanding the Basics, ASM International, 2013.
- 341 [24] A. Germak, A. Liguori, C. Origlia, Experience in the metrological characterization of primary hardness  
342 standard machines, in: Proceedings of HARDMEKO 2007, Tsukuba, Japan, November 19-21, 2007, pp. 81-  
343 89.
- 344 [25] A. Prato, D. Galliani, C. Origlia, A. Germak, A correction method for Vickers indenters squareness  
345 measurement due to the tilt of the pyramid axis, Measurement 140 (2019) 565-571.
- 346 [26] JCGM 100:2008, Evaluation of Measurement Data — Guide to the Expression of Uncertainty in Meas-  
347 urement (GUM), Joint Committee for Guides in Metrology, Sèvres, France.
- 348 [27] ISO/IEC 17043:2010, Conformity assessment - General requirements for proficiency testing. Interna-  
349 tional Organization for Standardization, Geneva, Switzerland.